Nanotechnology **20** (2009) 505703 (7pp) doi:10.1088/0957-4484/20/50/505703

'All-inclusive' imaging of the rutile TiO_2(110) surface using NC-AFM

Ralf Bechstein[1,4], **César González**[2], **Jens Schütte**[1,5], **Pavel Jelínek**[2], **Rubén Pérez**[3] **and Angelika Kühnle**[1,5]

[1] Fachbereich Physik, Universität Osnabrück, Barbarastraße 7, D-49076 Osnabrück, Germany
[2] Institute of Physics, Academy of Sciences of the Czech Republic, Cukrovarnická 10, 162 53 Prague, Czech Republic
[3] Departamento de Física Teórica de la Materia Condensada, Universidad Autónoma de Madrid, E-28049 Madrid, Spain

E-mail: ralf@inano.dk and ruben.perez@uam.es

Received 18 August 2009, in final form 2 October 2009
Published 19 November 2009
Online at stacks.iop.org/Nano/20/505703

Abstract

Non-contact atomic force microscopy (NC-AFM) at true atomic resolution is used to investigate the (110) surface of rutile TiO_2. We are able to *simultaneously* resolve both bridging oxygen and titanium atoms of this prototypical oxide surface. Furthermore, the characteristic defect species, i.e. bridging oxygen vacancies, single and double hydroxyls as well as subsurface defects, are identified in the very same frame. We employ density functional theory (DFT) calculations to obtain a comprehensive understanding of the relation between the tip apex structure and the observed image contrast. Our results provide insight into the physical mechanisms behind atomic-scale contrast, indicating that electrostatic interaction can lead to a far more complex contrast than commonly assumed.

(Some figures in this article are in colour only in the electronic version)

1. Introduction

Understanding the (110) surface of rutile titanium dioxide from direct visualization by scanning probe microscopy (SPM) techniques has been the focus of numerous publications in the last decade [1–10] as titania is generally regarded as 'an excellent model oxide' [6]. Identification of defect sites, surface reaction of water and oxygen, catalysis and molecular self-assembly have attracted considerable attention.

Usually, scanning tunneling microscopy (STM) senses the density of unoccupied states at titanium and defect sites [2]. Hence, the bridging oxygen atoms are invisible. Non-contact atomic force microscopy (NC-AFM) is known to be capable of imaging either the bridging oxygen atoms (hole mode) or the titanium atoms (protrusion mode) [5]. These contrast modes have been assigned to purely electrostatic interaction and do not, therefore, reflect the real topography of the surface. NC-AFM is sensing forces and does not, therefore, depend on the existence of adequate electronic states like in STM. However, imaging of all TiO_2(110) surface atoms at the same time has not been demonstrated so far with SPM.

Here, we study the (110) surface of rutile TiO_2 using NC-AFM and density functional theory (DFT). We present NC-AFM results revealing both bridging oxygen and titanium atoms *simultaneously*. Furthermore, oxygen vacancies, single and double hydroxyls, as well as further defects ascribed to subsurface impurities, are also unambiguously imaged within one single frame. These experimental results are supported by DFT calculations, unraveling details of the tip–sample interaction. Our work indicates that electrostatic interaction explains well simultaneous imaging of both bridging oxygen and titanium atoms when realistic tip models are taken into account.

The outline of the paper is as follows: first we present the experimental evidence for the appearance of the surface species in neutral and all-inclusive mode (section 2). Second we define a list of criteria the pair of tip models responsible for the observed contrast modes has to satisfy. In order to eventually identify the correct tip models we, then, present an extended search by means of first-principles calculations (section 3). We

[4] Present address: Interdisciplinary Nanoscience Center (iNANO), Department of Physics and Astronomy, Aarhus University, Ny Munkegade, DK-8000 Aarhus C, Denmark.
[5] Present address: Institut für Physikalische Chemie, Universität Mainz, Jakob-Welder-Weg 11, D-55099 Mainz, Germany.

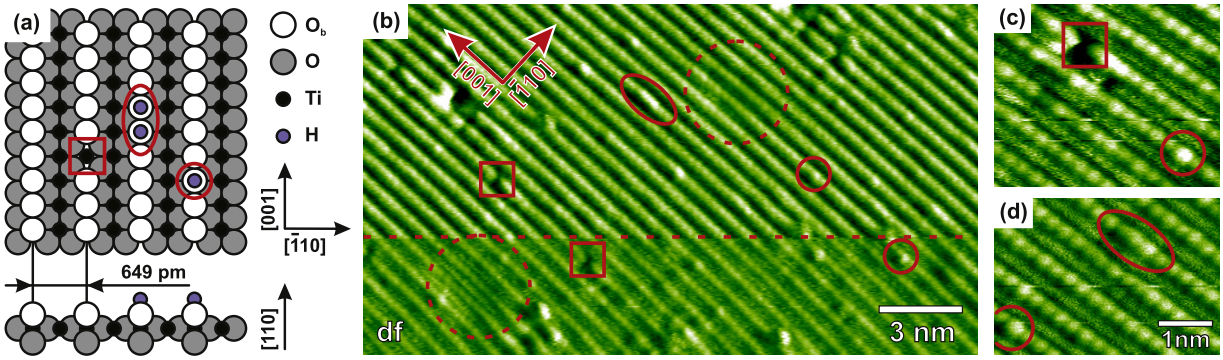

Figure 1. (a) Surface lattice structure of $TiO_2(110)$. Alternating rows of O_b and Ti atoms aligned along the [001] direction lead to the typical stripe-like pattern in SPM images. The dominant defect species on the surface are O_{vac}, and double and single OH as indicated by a square, ellipse and circle, respectively. A side view of an O–TiO–O tri-layer is shown below. In (b) a representative NC-AFM detuning image is shown, illustrating the appearance of the surface atoms and of the three defect species in neutral mode [12] (upper part) and all-inclusive mode (lower part). The contrast changes in the scan line indicated by the dashed line. Further defects assigned to subsurface impurities [13] are marked by dashed circles. (c) and (d) show detailed NC-AFM detuning images recorded in all-inclusive mode.

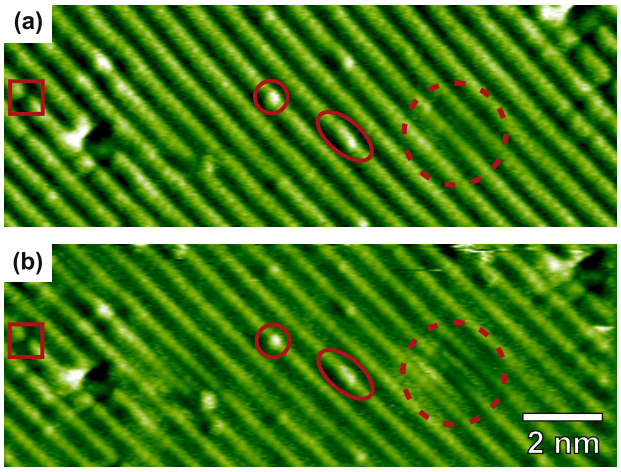

Figure 2. Consecutively obtained NC-AFM detuning images of rutile $TiO_2(110)$. Images (a) and (b) show the very same surface area in neutral and all-inclusive mode, respectively. Exemplary defects are marked in both images by a circle (single hydroxyl), oval (double hydroxyl), square (oxygen vacancy) and dashed circle (subsurface impurity).

will demonstrate that our proposed pair of tip models fulfill the listed criteria in a very satisfying way. Then, we discuss how the identified tip models give comprehensive insight into the nature of tip–sample interaction leading to a detailed understanding of the observed contrast modes (section 4). Finally, we present our conclusions (section 5).

2. NC-AFM experiments: 'all-inclusive' versus neutral imaging

Measurements were performed at room temperature in an ultra-high vacuum chamber with a base pressure lower than 1×10^{-10} mbar. The experimental set-up as well as TiO_2 sample preparation has been described elsewhere [11]. For NC-AFM measurements we used n-doped silicon cantilevers (NanoWorld, Neuchâtel, Switzerland) with a resonance frequency of about 300 kHz (type PPP-NCH) operated at an amplitude of about 10 nm. To remove contaminants the cantilevers were Ar^+-sputtered for 5 min at ion energies of 2 keV prior to use. The microscope was operated in the frequency-modulation mode. The shift of the eigenfrequency (detuning; df) was directly used as the imaging signal as the cantilever was scanned at a quasi-constant tip–surface distance. To minimize long-range electrostatic interactions, a bias voltage of about −1.1 V was applied to the tip. All images were taken with a scanning speed of 1 line s^{-1} and 500 pixel/line. All presented images are raw data images where bright colors correspond to highly attractive conservative interaction (detuning images) or highly dissipative interaction (dissipation image), respectively.

The surface structure of rutile $TiO_2(110)$ is depicted in figure 1(a). The three dominant defect species, namely oxygen vacancies (O_{vac}), double and single hydroxyls (OH), are exclusively situated in the bridging oxygen rows (O_b) [4]. In figure 1(b), an NC-AFM detuning image is shown. In the upper part, only the O_b rows are imaged as bright lines. In the lower part, the contrast has changed and additional faint, bright lines can be recognized in between the O_b rows. These lines can be assigned to the in-plane titanium rows (Ti). Thus, this image is the first SPM image showing both O_b and Ti rows simultaneously. Consequently, we introduce this contrast as an 'all-inclusive' mode. In figures 1(c) and (d), all-inclusive mode images are presented, showing the appearance of all surface atoms in detail.

The dominating defect species in figure 1(b) are circular and elongated protrusions as well as holes, situated in bright O_b rows, assigned to single and double OH as well as O_{vac}, respectively. Protruding defects in bright O_b rows have been reported before and assigned to a neutral tip [12]. Here, we present a neutral mode image (upper part of figure 1(b)) containing all three defect species, unraveling the appearance of O_{vac} sites in the neutral mode. While single and double OH appear to protrude into the bright O_b rows, O_{vac} sites appear as holes. The essential difference between the neutral and the all-inclusive mode is the additional appearance of the Ti atoms as faint bright rows in the all-inclusive mode.

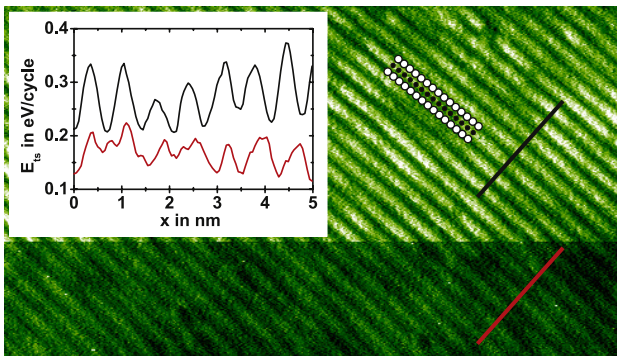

Figure 3. NC-AFM dissipation image corresponding to the detuning image presented in figure 1(b). The titanium rows appear bright which denotes higher dissipation at titanium sites compared to bridging oxygen sites. The line profiles depict the site-specific energy dissipated in each oscillation cycle due to tip–sample interaction E_{ts} in 'all-inclusive' mode (red line) and neutral (black line) mode. The dissipation of the freely oscillating cantilever was measured to be (2.8 ± 0.2) eV per oscillation cycle, while the detection limit is about 15 meV.

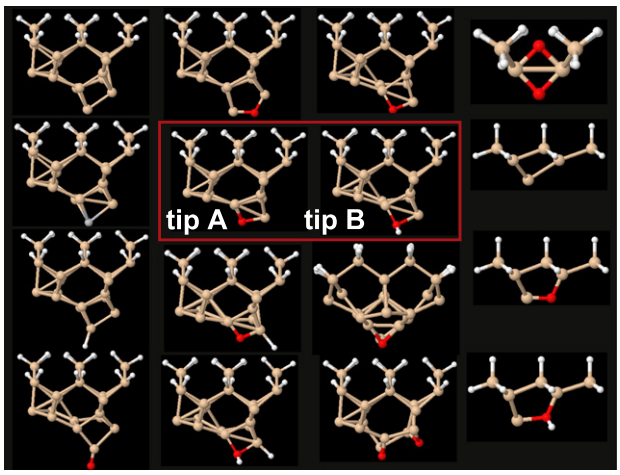

Figure 4. Schematic view of all stable tip models. We use Si-based clusters, with the upper layers passivated with hydrogens (represented by white balls), and include possible contamination at the apex with different impurities: H, Ti (gray) and O (red). Most of the tips are built up on (100) surface orientation, but the last three tips in the fourth column are (111)-oriented.

A direct comparison of the very same surface area in neutral and all-inclusive mode is presented in figure 2. Figure 2(a) shows an image taken in the neutral mode, exhibiting single and double hydroxyls, oxygen vacancy and subsurface impurity in one single frame. After a tip change, this surface area is imaged in the all-inclusive mode (figure 2(b)), allowing for a direct comparison of titanium and bridging oxygen row sites as well as all defect species in the neutral and all-inclusive mode, respectively. The direct observation of contrast changes and the detailed knowledge of the detuning at all surface sites in both modes allows us to compare the experimental findings with DFT simulations.

We repeatedly obtained the highest-resolution images in neutral, 'all-inclusive', hole and protrusion mode with NC-AFM on $TiO_2(110)$. In the simple majority of all experiments the surface was imaged in neutral mode but usually more than one contrast mode was observed during each experiment. The vast majority of experiments did not show 'all-inclusive' contrast. We furthermore observed contrast changes between all four contrast modes even during one single experiment. All contrast changes were unintended and randomly occurring events. We never tried to change the contrast mode in a controlled way but rather aimed at stable imaging conditions. In our experience, contrast changes between neutral mode and hole mode or protrusion mode constituted rare events that resulted from dramatic changes in the tip apex and led from one persistent configuration to another. Those events usually appeared as 'tip crash' with sudden and strong dissipative interaction and a jump in the tip–sample distance. In contrast, contrast changes between neutral mode and 'all-inclusive' mode occurred frequently and reversibly without tip crash. The frequency of contrast changes between neutral mode and 'all-inclusive' mode was observed to range from none in several hours up to a few per minute. In total, we observed several tens of contrast changes from neutral mode to 'all-inclusive' mode and vice versa. None of them coincided with a significant change in tip–sample distance. The typical change in dissipation was as small as 100 meV (see figure 3). From these observations two conclusions can be drawn. First, the neutral tip as well as the 'all-inclusive' tip allow for stable imaging. Second, both tips have to be related by a very likely, simple and reversible transition.

The absolute detuning values at various surface sites in the particular experiment presented here are in the range of -50 to -70 Hz. However, the corrugation is less than 20 Hz. Thus, the main contribution to the detuning is very likely due to long-range interaction which is specific for the macroscopic shape of the particular tip but of less importance for the comparison of the two contrast modes. To eventually separate the detuning due to site-specific short-range interaction from the overall detuning offset, the distance-dependent detuning corrugation was analyzed. The typical row structure of the $TiO_2(110)$ surface was first observed after an increase of the detuning to about -50 Hz. Thus, the detuning due to long-range interaction can be estimated to be at least -50 Hz. Hence, the detuning values measured in this experiment (see also table 1) were corrected for this offset.

3. *Ab initio* calculations: unraveling the tip apex structure

To understand in detail the mechanism responsible for the observed contrasts in neutral and all-inclusive mode and the frequent contrast changes, we have performed an extensive search for reliable tip models.

We have considered a large variety of atomic models of silicon-based tips that vary in structure, composition, termination and relative orientation with respect to the surface. The 16 most promising candidates are shown in figure 4. Each of the model tips were under consideration for explaining one of the observed contrast modes. Thus, the 16 tip models depicted in figure 4 correspond to 136 possible pairs of tip

Table 1. Summary of the experimental and calculated (in parentheses) detuning for both neutral and all-inclusive mode at a tip–sample distance of 3.4 Å over different surface sites. For direct comparison between experimental and theoretical data we have subtracted from the experimental data the estimated detuning due to long-range interaction of −50 Hz. The error of the experimental detuning values is 1 Hz.

	All-inclusive mode (tip A) df in Hz	Neutral mode (tip B) df in Hz
Ti	−11(−9)	−3(−4)
O_b	−15(−11)	−15(−11)
Ti–O_b	4(2)	12(7)
O_{vac}	−7(−12)	−8(−3)
OH	−18(−34)	−20(−22)

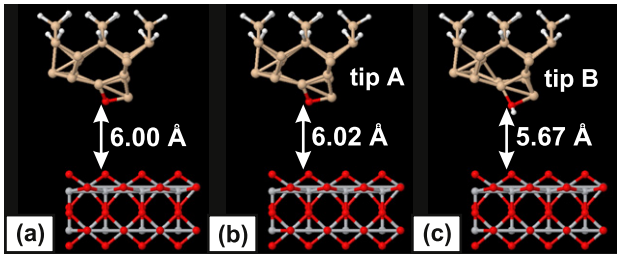

Figure 5. Definition of the tip–sample distance in the DFT calculations. The distance is measured with respect to the fixed layers in the tip and sample in order to mimic the constant piezodisplacement in the experiment. With an appropriate choice for the reference, it corresponds, in the absence of relaxations, to the height difference between the apex oxygen atom of the all-inclusive tip A and the outermost O_b row (a); (b) and (c) show the real height difference after the relaxation for the all-inclusive tip A and the neutral mode tip B. Notice that the topmost layers of both tips are located at the same height to mimic the constant-height mode used in the experiments. A tip–sample distance of 3.4 Å as discussed in the text corresponds to approaching the topmost layer of both tips by 2.6 Å towards the surface.

models. To eventually identify the right tips we hereby define a list of criteria which needs to be fulfilled by the correct pair of tip models. (i) The tip structure should be mechanically stable, as stable imaging in both modes was possible. The tip models have to be composed of silicon atoms as this is the material the cantilever is made of. The tip apex might be contaminated with titanium, oxygen and/or hydrogen. Given the excellent base pressure in the AFM chamber, other contaminations have to be considered rather unlikely. (ii) The large number of observed switches between the two contrast modes must be reflected by a pair of tip models that are related by a simple change of the tip apex termination involving only a few atoms. (iii) The tips should reproduce the correct detuning values at O_b and Ti sites in both contrast modes. The detuning at O_b sites should be identical with both tips, while the interaction with Ti needs to be different. (iv) The model for the all-inclusive tip has to provide atomic resolution resolving both rows according to the experimental evidence while the model of the neutral tip does not. (v) The tips should reproduce the correct detuning values at defect sites in both contrast modes. In particular, the fact that OH groups appear brighter than O_b sites while O_{vac} sites are imaged as depressions has to be reproduced with both tips.

Calculations of the tip–surface interaction for all tip models were carried out with a local basis set DFT code, FIREBALL [14], designed to deal with large-scale simulations while offering a very favorable accuracy–efficiency balance [15]. Here, we use a double numerical (DN) basis set including s-orbitals for H (cutoff radius $R_c(s) = 3.8$ au); a DN basis set with s-, p-orbitals ($R_c(s) = 3.3$ au and $R_c(p) = 3.8$ au) for O; a single numerical s, p basis set ($R_c(s) = 4.8$ au and $R_c(p) = 5.4$ au) for Si and an s, p, d basis set for Ti ($R_c(s) = 6.2$ au, $R_c(p) = 6.7$ au and $R_c(d) = 5.7$ au). These basis sets give very good descriptions of both, TiO_2 bulk and the $TiO_2(110)$ surface. The Si basis set has been successfully used in previous works [16]. The surface was modeled by a (4 × 3) slab with a thickness of 2 tri-layers (see figure 1(a)) containing 144 atoms. Four k-points were used to sample the Brillouin zone. To simulate the tip–sample interaction, we have subsequently approached the different tips in a quasi-static manner, with $\Delta z = 0.25$ Å ($\Delta z = 0.1$ Å for the final pair), to the surface at zero temperature. The tip–sample distance in the simulations is measured with respect to the fixed layers in the tip and sample as depicted in figure 5 and thus is consistent with the piezodisplacement in the experiments carried out in a constant-height manner.

The 60 atoms in the bottom slab layer and the topmost part of the tip model were kept fixed in their ideal configuration. The atomic positions at each step were relaxed until the total energy and forces were converged to 10^{-6} eV and 0.05 eV Å^{-1}, respectively. The theoretical detuning corresponding to the short-range force was obtained using standard analytic formulae as given in equation 5.9 in [17]. Test calculations with selected tips on a (4 × 3) slab with three tri-layers and a (5 × 3) slab with two tri-layers did not show any significant modifications of the force curves.

We will now address the application of our list of criteria for reliable tips introduced above to identify the right tips among those shown in figure 4. To fulfill criterion (i), the tips were modeled by two different Si-based clusters built upon (111) and (100) surface orientations [18]. The top layers are passivated with hydrogens, while the apices include reliable contaminations with different impurities (Ti, O, H). The mechanical stability of each tip model was tested performing an approach/retraction curve on an Si cluster reaching the maximum of the attractive force. Only the tips whose structure remained intact after this process were considered in our DFT study. Among all these stable models, the tips labeled A and B in figure 4 constitute the very tip pair that best fulfills all of our criteria for reliable tip models as discussed in the following. Both tips share the same basic atomic structure, derived from a (100)-oriented Si tip with a dimer-like termination [19] oriented parallel to the O_b rows. The only difference is the nature of the apex: an O atom in tip A and an OH group for tip B. The structural transition between those two tips involves a relatively simple process of adsorption/desorption nature of a single hydrogen, which can be expected to take place in the experiment and, therefore, satisfies very well our criterion (ii).

The selected tip pair also matches very nicely criterion (iii). The tips reproduce the correct detuning values at

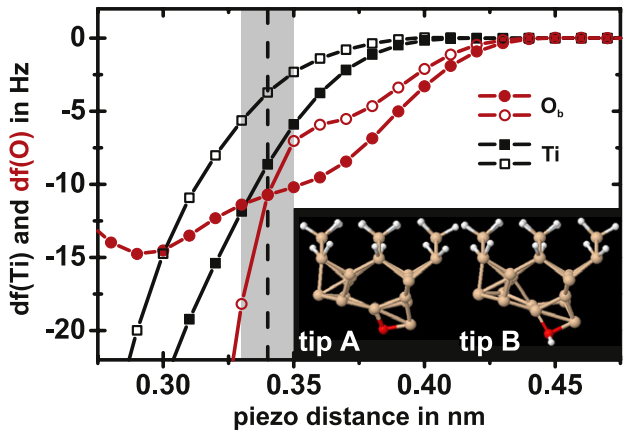

Figure 6. Theoretical df–distance curves over O_b (circles) and Ti (rectangles) sites obtained with all-inclusive tip A (full symbols) and neutral mode tip B (empty symbols). The vertical dashed line represents the tip–sample distance of 3.4 Å, where the theoretical corrugation matches the experimental results (gray box indicates experimental error). For distance definition see figure 5. The error of the calculated detuning values is smaller than the size of the symbols.

O_b and Ti sites in both contrast modes. Figure 6 shows the detuning–distance curves over O_b and Ti sites obtained with tip A and tip B. Both tips show identical detuning at the O_b site at 3.4 Å, as experimentally observed. As the topmost layers of both tips are always located at the very same height in our simulation to mimic the constant-height mode, a tip–sample distance of 3.4 Å corresponds to approaching the topmost layer of both tips by 2.6 Å towards the surface (see also figure 5). At the very same distance tip A reproduces very well the experimental detuning observed in the all-inclusive mode while tip B reproduces the observed detuning in neutral mode (for absolute values see table 1). In particular, the theoretical detuning corrugation between the Ti and O_b site is +2 Hz with tip A, very close to the experimental one (4 ± 2) Hz (all-inclusive mode). At the same tip–sample distance, tip B gives a detuning corrugation of +7 Hz, nicely reproducing the experimental value, (12 ± 2) Hz, acquired in the neutral mode (see also figures 7(c) and (f)).

Moreover, tip A meets criterion (iv) in providing atomic resolution and resolving both O_b and Ti rows simultaneously, as demonstrated in the simulated detuning image shown in figure 7(d). This image, calculated at a tip–sample distance of 3.4 Å, clearly shows that tip A is capable of resolving both bright O_b atoms and less distinct Ti atoms, in excellent agreement with the experiment (figure 7(a)). Figure 7(e) shows a simulated image that is calculated at the same tip–sample distance of 3.4 Å using the neutral tip model tip B. The image clearly shows that the simultaneous resolution of O_b and Ti rows is not possible with tip B although the apex of the model appears sharper than that of tip A.

Our theoretical predictions using the all-inclusive tip A and the neutral mode tip B for the same distance (see table 1) show the OH groups as the most reactive site in both imaging modes as observed experimentally. Although well-known theoretical difficulties to deal with oxygen vacancies on the rutile TiO_2 surface exist (see, e.g., [20]), we have found that the O_{vac} is at least not brighter than the O_b row using both tip models, and shows a contrast similar to the Ti atoms, qualitatively reproducing experimental findings. Therefore, we can conclude that our tip pair also matches criterion (v).

4. Discussion: understanding the image contrast

In order to understand the contrast formation in neutral and all-inclusive modes, we have to consider how the structure and composition of both tips control the nature of the tip–sample interaction. Our calculations show that the relative contribution of the weak short-range electrostatic interaction [21, 22] and the onset of chemical bonding between the closest tip and surface atoms [16, 22, 23] is very sensitive to the tip–sample distance, defining different interaction regimes. Thus, we have focused our analysis of the electronic structure and charge distribution on the distance around 3.4 Å, where the theory matches the experimental detuning corrugation.

A global charge transfer from the tip to the surface due to the Fermi level alignment between tip and sample exists at large distances. This has been already identified in a previous study for an Si tip [22, 24]. Nevertheless, this charge excess distributes over the whole sample and, therefore, provides a background force that does not contribute to the image contrast and is most likely compensated by the bias voltage that was applied to the tip in the experiment.

We have not found a significant difference in the atomic Löwdin charges[6] between the atom closest to the tip and other equivalent surface atoms. Moreover, there is no noteworthy overlap between the tip and surface electron densities, as can clearly be seen in figure 8. These two facts seem to rule out the formation of a strong covalent bond between tip and sample, leaving the short-range electrostatic forces as the component dominating the tip–sample interaction.

So far, the NC-AFM image contrast on ionic surfaces has been interpreted in terms of the tip polarity. It has been assumed that the tip polarity and, hence, the imaging contrast is controlled by the nature of the last atom at the apex [25]. According to this simple idea, we would expect the negatively terminated tip A to feel a repulsive interaction over the O_b sites inducing a larger image contrast over the Ti atoms, and tip B to behave as a positive tip imaging preferentially the O_b sites and not the OH defects. Our calculations, where both tips A and B provide a larger attractive interaction over the O_b sites, show that the situation is far more complicated.

The mobility of the H atom in tip B, which controls the screening of the negatively charged oxygen atom, explains the ability of tip B to interact with both the O_b atoms and the OH defects (see figures 8(d) and (f)). This results in the so-called neutral contrast mode [12] reflecting the surface topography. Further evidence for the existence of a mobile species at the apex of tip B that is missing at the apex of tip A is provided by the dissipation signal (figure 3) that shows higher dissipation

[6] Our discussion of the charge transfer associated with the tip–sample interactions is based on a projection of the total charge distribution into a local orbital basis. To define these atomic charges, we favor the Löwdin scheme, which does not suffer from the overlap problem, particularly important at close tip–surface distances, of the Mulliken analysis.

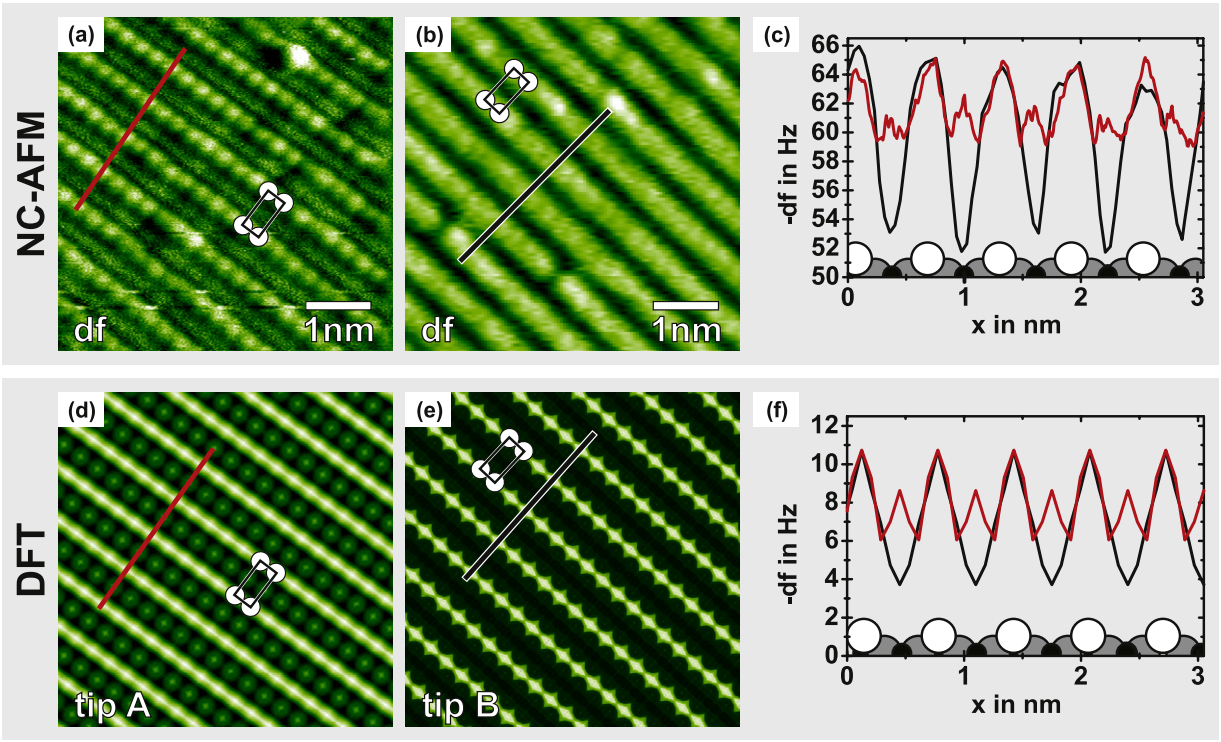

Figure 7. Measured (a)–(c) and simulated (d)–(f) detuning data of the rutile TiO_2(110) surface in both all-inclusive mode ((a), (d) and red lines) and neutral mode ((b), (e) and black lines). Theoretical images using the proposed pair of tip models reproduce nicely the observed contrast modes. Furthermore, detuning line profiles perpendicular to the O_b rows show very good quantitative agreement between theory and experiment. Note that the calculations do not include van der Waals interaction. However, the long-range interaction does not provide atomic-scale contrast but adds a constant background of about −50 Hz to the experimental images.

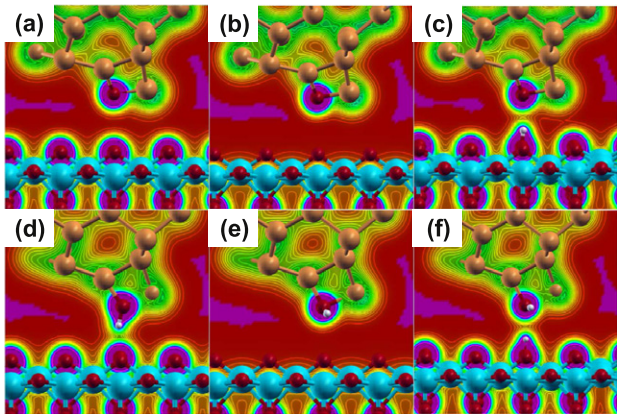

Figure 8. Projected electron density using two different models: the all-inclusive tip A (a)–(c) and the neutral mode tip B (d)–(f) at the distance of 3.4 Å. The plots depict a plane normal to the surface and passing through the apex dimer for vertical scans over surface O_b ((a) and (d)), Ti ((b) and (e)) and OH site ((c) and (f)). The figures do not show a significant overlap between the tip and surface electron densities at a distance of 3.4 Å. This fact seems to rule out the presence of a strong chemical bond between tip and sample.

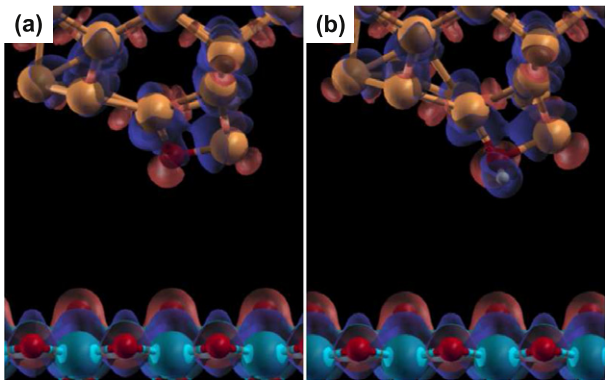

Figure 9. Differential electron density (obtained by subtracting the sum of atomic charge densities from the total charge density) for the all-inclusive tip A (a) and the neutral tip B (b) at a distance of 5.00 Å. Red color represents an excess of the electronic charge density, while blue indicates a depletion of the electronic charge. The charge redistribution at a distance of 3.40 Å, where the theoretical corrugation matches the experiment, practically does not differ from the one shown here.

and higher dissipation contrast in the neutral mode compared to the 'all-inclusive' mode. Furthermore, figure 3 clearly indicates that higher dissipation is measured at titanium sites implying that, indeed, the hydrogen at the apex of tip B bends towards the neighboring bridging oxygen row when the tip is above a titanium site. This effect is much more pronounced in neutral mode while the dissipation contrast in 'all-inclusive' mode is barely larger than the detection limit.

The case of tip A is even more subtle. The attractive interaction over the O_b sites originates from a delicate balance between the O–O repulsion and the attractive interaction of the Si atom in the apex dimer with the adjacent atom in the O_b row. Figure 9 shows the differential electron density obtained

by subtracting the sum of atomic charge densities from the total charge density for both tip models. The plots show an intricate redistribution of electronic charges on the tip apices that are far from an atomic point charge picture. The complex inhomogeneous charge redistribution around the apex atoms requires a precise integration of the charge distribution to evaluate accurately the short-range electrostatic force between tip and sample. Both the value of the effective charges and their spatial extension have to be taken into account in the accurate evaluation of the electrostatic force, as we do in the present study, to capture the effect of simultaneous imaging of O_b as well as Ti rows.

5. Conclusion

In conclusion, we have presented high-resolution NC-AFM images of rutile $TiO_2(110)$, revealing both O_b atoms as well as Ti rows *simultaneously*. Furthermore, the characteristic defects of this surface can be identified in the very same frame. Based on DFT calculations, we have identified a pair of apex tip models, which perfectly reproduce the experimental detuning contrast. Moreover, this pair of tips provide a simple explanation for the frequent contrast changes observed in experiment. Our results reveal that even simple tip apex structures may result in far more complex electrostatic interactions than assumed so far.

Acknowledgments

Financial support from the DFG (ENP) is gratefully acknowledged (RB, JS and AK). The work was supported by grant nos. GAAV IAA100100905, AV0Z10100521 and 2008CZ0025 (PJ and CG) as well as projects MAT2008-02929/NAN and MAT2008-02953-E (RP) and grant 2007-0034 (CG) of the Spanish Ministerio de Ciencia e Innovación. Computer time provided by the Spanish Supercomputing Network (RES) is gratefully acknowledged.

References

[1] Fukui K-I, Onishi H and Iwasawa Y 1997 *Phys. Rev. Lett.* **79** 4202
[2] Diebold U *et al* 1996 *Phys. Rev. Lett.* **77** 1322
[3] Diebold U 2003 *Surf. Sci. Rep.* **48** 53
[4] Wendt S *et al* 2005 *Surf. Sci.* **598** 226
[5] Lauritsen J V *et al* 2006 *Nanotechnology* **17** 3436
[6] Bowker M 2006 *Curr. Opin. Solid State Mater. Sci.* **10** 153
[7] Zhang Z *et al* 2006 *J. Phys. Chem.* B **110** 21840
[8] Bikondoa O *et al* 2006 *Nat. Mater.* **5** 189
[9] Wendt S *et al* 2008 *Science* **320** 1755
[10] Pang C L, Lindsay R and Thornton G 2008 *Chem. Rev. Soc.* **37** 2328
[11] Schütte J *et al* 2008 *Phys. Rev.* B **79** 045428
[12] Enevoldsen G H *et al* 2007 *Phys. Rev.* B **76** 205415
[13] Batzill M *et al* 2002 *Phys. Rev.* B **66** 235401
[14] Jelinek P *et al* 2005 *Phys. Rev.* B **71** 235101
[15] Basanta M A *et al* 2007 *Comput. Mater. Sci.* **39** 759
[16] Sugimoto Y *et al* 2007 *Nature* **446** 64
[17] Garcia R and Pérez R 2002 *Surf. Sci. Rep.* **47** 197
[18] Pou P *et al* 2009 *Nanotechnology* **20** 264015
[19] Oyabu N *et al* 2006 *Phys. Rev. Lett.* **96** 106101
[20] Morgan B J and Watson G W 2007 *Surf. Sci.* **601** 5034
[21] Lantz M A *et al* 2003 *Phys. Rev.* B **68** 035324
[22] Foster A S *et al* 2003 *Phys. Rev.* B **68** 195420
[23] Pérez R *et al* 1998 *Phys. Rev.* B **58** 10835
[24] Foster A S *et al* 2004 *Phys. Rev. Lett.* **92** 036101
[25] Enevoldsen G H *et al* 2008 *Phys. Rev.* B **78** 045416